

RHESSI and SOHO/CDS Observations of Explosive Chromospheric Evaporation

Ryan O. Milligan^{1,3}, Peter T. Gallagher^{2,3,4}, Mihalis Mathioudakis¹, Francis P. Keenan¹,
and Richard A. Schwartz^{3,5}

ABSTRACT

Simultaneous observations of explosive chromospheric evaporation are presented using data from the *Reuven Ramaty High Energy Solar Spectroscopic Imager (RHESSI)* and the Coronal Diagnostic Spectrometer (CDS) onboard *SOHO*. For the first time, co-spatial imaging and spectroscopy have been used to observe explosive evaporation within Hard X-Ray footpoints. *RHESSI* X-ray images and spectra were used to determine the flux of non-thermal electrons accelerated during the impulsive phase of an M2.2 flare. Assuming a thick-target model, the injected electron spectrum was found to have a spectral index of ~ 7.3 , a low energy cut-off of ~ 21 keV, and a resulting flux of $\geq 3 \times 10^{10}$ ergs $\text{cm}^{-2} \text{s}^{-1}$. The dynamic response of the atmosphere was determined using CDS spectra, finding upflow velocities of 270 ± 28 km s^{-1} in Fe XIX (592.23 Å), and associated downflows of 30 ± 15 km s^{-1} at chromospheric and transition region temperatures. The properties of the accelerated electron spectrum and the corresponding evaporative velocities were found to be consistent with the predictions of theory.

Subject headings: Sun: atmospheric motions – Sun: flares – Sun: UV radiation – Sun: X-rays, γ rays

1. INTRODUCTION

Current solar flare models (Antiochos & Sturrock 1978; Fisher, Canfield & McClymont 1984, 1985a,b,c; Mariska, Emslie, & Li 1989) predict two types of chromospheric evaporation processes. “Gentle” evaporation occurs when the chromosphere is heated either directly by non-thermal electrons, or indirectly by thermal conduction. The chromospheric plasma subsequently loses energy via a combination of radiation and low-velocity hydrodynamic expansion. “Explosive” evaporation takes place when the chromosphere is unable to radiate energy at a sufficient rate and

consequently expands at high velocities into the overlying flare loops. The overpressure of evaporated material also drives low-velocity downward motions into the underlying chromosphere, in a process known as chromospheric condensation.

From a theoretical perspective, Fisher, Canfield & McClymont (1985a) investigated the relationship between the flux of non-thermal electrons (F), and the velocity response of the chromosphere for the two classes of evaporation. For gentle evaporation, non-thermal electrons fluxes of $\leq 10^{10}$ ergs $\text{cm}^{-2} \text{s}^{-1}$ were found to produce upflow velocities of tens of kilometres per second. In contrast, explosive evaporation was found to be associated with higher non-thermal electron fluxes ($F \geq 3 \times 10^{10}$ ergs $\text{cm}^{-2} \text{s}^{-1}$), which drive both upflows of hot material at velocities of several hundred kilometres per second *and* downflows of cooler material at several tens of kilometres per second.

Observationally, previous studies have identified blue-shifted Soft X-Ray (SXR) and EUV lines indicative of chromospheric evaporation. Using

¹Department of Physics and Astronomy, Queen’s University Belfast, Belfast, BT7 1NN, Northern Ireland.

²School of Physics, University College Dublin, Belfield, Dublin 4, Ireland.

³Laboratory for Astronomy and Solar Physics, NASA Goddard Space Flight Center, Greenbelt, MD 20771, U.S.A.

⁴L-3 Communications GSI.

⁵Science Systems and Applications, Inc.

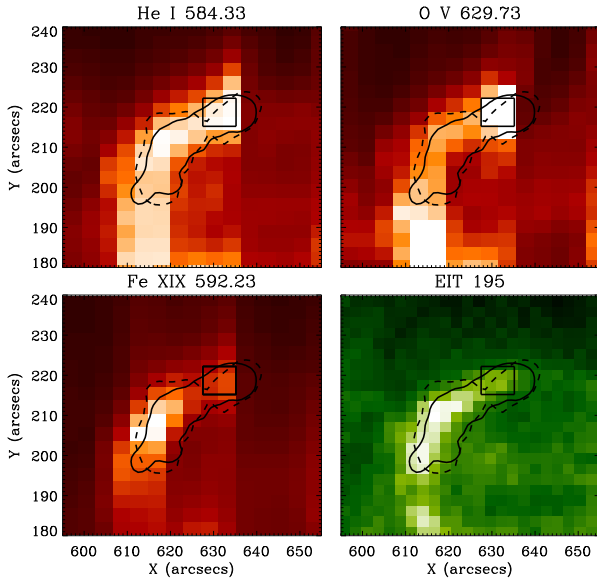


Fig. 1.— CDS images in the He I, O V, and Fe XIX emission lines observed during the impulsive phase of the flare, with the corresponding EIT 195 Å image. *RHESSI* 12–25 keV (*dashed*) and 25–60 keV (*solid*) contours are overlaid, drawn at 10% and 20% of the peak intensity, respectively. The box centered at (631'', 218'') indicates the 2×2 pixel area over which the CDS spectra were integrated.

the Bent Crystal Spectrometer onboard the *Solar Maximum Mission*, Antonucci & Dennis (1983) and Zarro & Lemen (1988) reported upflow velocities of 400 km s⁻¹ and 350 km s⁻¹, respectively, in Ca XIX lines (3.1–3.2 Å). More recently, Czakowska et al. (1999) and Teriaca et al. (2003) observed velocities of 150–200 km s⁻¹ in Fe XIX (592.23 Å), using the Coronal Diagnostic Spectrometer (CDS; Harrison et al. 1995) onboard the *Solar and Heliospheric Observatory (SOHO)*. While these studies provided a measurement of the dynamic response of the flaring chromosphere, they were unable to provide a measurement of the flux of electrons responsible for driving such motions, nor the spatial relationship between the two.

In this *Letter*, simultaneous *Reuven Ramaty High Energy Solar Spectroscopic Imager (RHESSI)*; Lin et al. 2002) and CDS observations are combined for the first time to investigate the relationship between the non-thermal electron flux and the response of the solar atmosphere. In Section 2 the

analysis techniques employed are described, while the results are presented in Section 3. Our Conclusions are then given Section 4.

2. OBSERVATIONS AND DATA ANALYSIS

This study focuses on a *GOES* M2.2 flare, which began at 12:44 UT on 2003 June 10. The event was selected from a sample of approximately 50 flares jointly observed by *RHESSI* and CDS. The limited field of view, cadence, and operating schedule of CDS, coupled with *RHESSI* nighttime and South Atlantic Anomaly passes, make simultaneous observations by the two instruments quite rare.

The CDS observations reported here were obtained with the *FLARE_AR* observing sequence. *FLARE_AR* contains five $\lesssim 4$ Å wide spectral windows centered on He I (584.33 Å; log T = 4.5), O V (629.73 Å; log T = 5.4), Mg X (624.94 Å; log T = 6.1), Fe XVI (360.76 Å; log T = 6.4), and Fe XIX (592.23 Å; log T = 6.9). Each raster consists of 45 slit positions, each ~ 15 seconds long (including the time it takes to move the slit), resulting in an effective cadence of ~ 11 minutes. The slit itself is 4''×180'' resulting in a $\sim 180'' \times 180''$ field of view. A zoomed-in region of the He I, O V, and Fe XIX rasters from the impulsive phase of the flare (from 12:45:20–12:55:42 UT) is given in Figure 1. Also shown is the Extreme ultraviolet Imaging Telescope (EIT; Delaboudiniere et al. 1995) 195 Å passband image obtained at 12:48 UT.

Each of the five CDS lines were extracted from a 2×2 pixel area centred on (631'', 218''), corresponding to a time interval of 12:47:50 – 12:48:20 UT. This position was chosen due to an O V brightening within the Hard X-Ray (HXR) contour which implied possible footpoint emission and is denoted by the box in Figure 1. These lines were then fitted with broadened Gaussian profiles (Thompson 1999), with Doppler shifts measured relative to quiet-Sun spectra. Preliminary fits to the Fe XIX line revealed that it was broadened beyond the instrumental resolution. As the profile appeared to have a blue asymmetry the possibility of line-blending was investigated but eliminated (G. del Zanna 2005, private communication). Figure 2 shows the Fe XIX (592.23 Å) line observed integrated over this area. The best fit to the line was consistent with stationary and blue-shifted

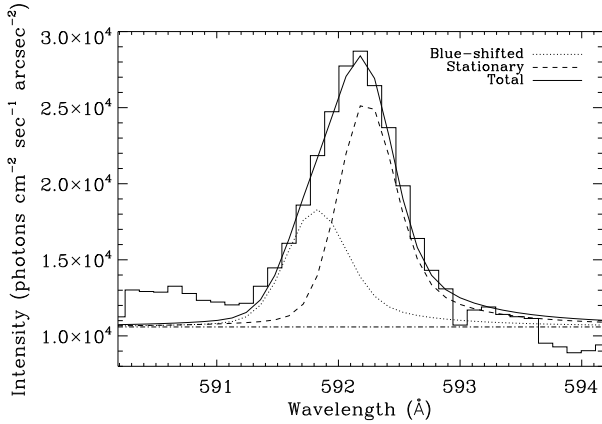


Fig. 2.— The Fe XIX line profile summed over the 2×2 pixel area centered on $(631'', 218'')$. The *dashed* line indicates the stationary component at 592.23 \AA , while the *dotted* line shows the blue-shifted component at 591.81 \AA . The flux of the blue-shifted component was found to be $\sim 50\%$ of that of the stationary component.

components with widths similar to the instrumental resolution. As Fe XIX is not observed in quiet-Sun spectra, and following from Teriaca et al. (2003), the Doppler velocity was measured as the shift between these two components. Due to the longitude of the observations and assuming purely radial flows, a heliographic correction was also applied.

RHESSI is an imaging spectrometer capable of observing X- and γ -ray emission over a wide range of energies ($\sim 3 \text{ keV}$ – 17 MeV). During this event the thin attenuators on *RHESSI* were in place (A1 state), thus limiting the energy range to $\gtrsim 6 \text{ keV}$. Flare emission was not observed at energies above $\sim 60 \text{ keV}$. The flare lightcurves are shown in the top panel of Figure 3. Both the *RHESSI* images and spectra were obtained over a 32 second period from 12:47:50–12:48:22 UT to coincide with the timerange over which the CDS spectra were extracted (to the nearest integer number of spacecraft rotations). This time interval lies within the 25–60 keV HXR burst and is indicated by two vertical dotted lines in the top panel of Figure 3.

RHESSI images in two energy bands (12–25 and 25–60 keV) were reconstructed using the *Pixon* algorithm (Hurford et al. 2002). Contours at 10%

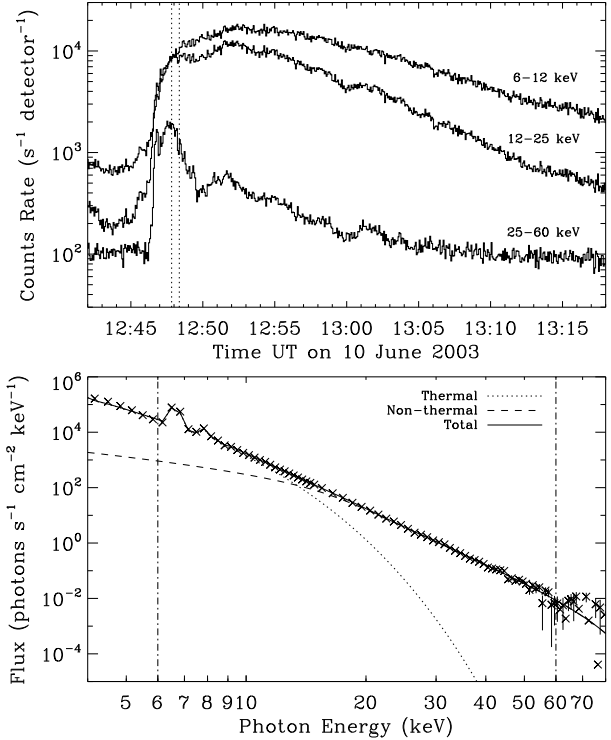


Fig. 3.— *Top panel:* *RHESSI* lightcurves from the 6–12, 12–25, and 25–60 keV bands. The dotted vertical lines indicate the time interval over which images and spectra were obtained to correspond to the CDS observations. *Bottom panel:* Portion of the *RHESSI* spectrum integrated over the timerange given above. The energy range 6–60 keV (vertical dot-dash lines) was fitted with an isothermal component (*dotted curve*) and a thick-target bremsstrahlung component (*dashed curve*).

and 20% of the peak intensity, respectively, in each band are overlaid on each EUV image in Figure 1. The 25–60 keV contour in particular overlies the bright kernel seen in O V. The *RHESSI* spectrum was fitted assuming an isothermal distribution at low energies, and thick-target emission at higher energies (Holman 2003; bottom panel of Figure 3). The total power of non-thermal electrons above the low energy cut-off (ϵ_c) was then calculated from $P(\epsilon \geq \epsilon_c) = \int_{\epsilon_c}^{\infty} f_e(\epsilon) d\epsilon \text{ ergs s}^{-1}$, where $f_e(\epsilon) \sim \epsilon^{-\delta}$ electrons $\text{keV}^{-1} \text{ s}^{-1}$ is the thick-target electron injection spectrum and δ is the associated spectral index (Brown 1971). Following

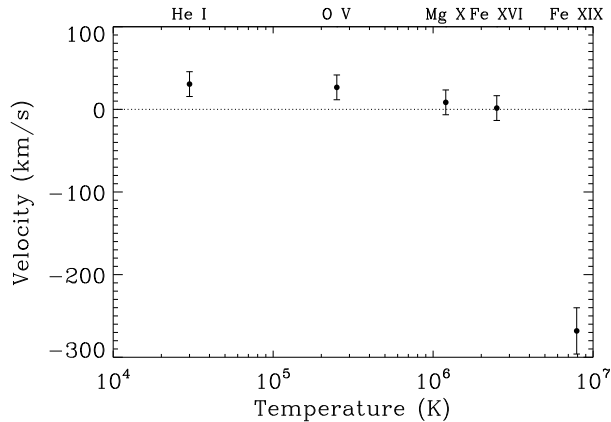


Fig. 4.— Plasma velocity as a function of temperature for the five lines observed using CDS. Positive velocities indicate downflows, while negative values indicate upflows. Error bars represent 1σ uncertainties.

Phillips (2004), the thermal component was further constrained by an analysis of the equivalent width of the Fe line complex at ~ 6.7 keV. The remaining flux was assumed to be from radiating non-thermal electrons which are responsible for driving chromospheric evaporation.

3. RESULTS

The thick-target model fitted to the *RHESSI* spectrum in Figure 3 was consistent with an electron distribution having $\epsilon_c \sim 21$ keV and $\delta \sim 7.3$. The total power in non-thermal electrons was therefore 5×10^{28} ergs s^{-1} . Using the reconstructed images, the 25–60 keV source area was calculated by summing over all pixels with counts greater than 20% of the peak value. A threshold of 20% was chosen to eliminate sources outside of the main HXR-emitting region, which were assumed to be unreal; the source area was not found to be highly sensitive to this threshold. Assuming a filling factor of unity, an upper-limit to the HXR source size was thus found to be 2×10^{18} cm², resulting in a non-thermal electron flux of $\geq 3 \times 10^{10}$ ergs cm⁻² s⁻¹. This area was also confirmed using the Fourier modulation profiles from each of *RHESSI*'s nine detectors, which are sensitive to spatial scales from 2.2'' to 183''.

Figure 4 shows plasma velocities as a function of

temperature for each of the five CDS lines using the methods described in Section 2. At chromospheric and transition region temperatures, plasma velocities show red-shifts of 30 ± 15 km s^{-1} with respect to quiet-Sun values, while the blue-shift observed in the 8 MK Fe XIX line corresponds to a velocity of 270 ± 28 km s^{-1} . No significant flows were observed in the Mg X and Fe XVI lines. The combination of high-velocity upflows and low-velocity downflows, together with a non-thermal electron flux of $\geq 3 \times 10^{10}$ ergs cm⁻² s⁻¹ provides clear evidence for explosive chromospheric evaporation.

4. DISCUSSION AND CONCLUSIONS

For the first time, simultaneous HXR and EUV observations of chromospheric evaporation are presented using *RHESSI* and *SOHO/CDS*. High velocity upflows (~ 270 km s^{-1}) were clearly observed in high-temperature Fe XIX emission during the impulsive phase of an M2.2 flare, while much lower downflow velocities (~ 30 km s^{-1}) were observed in the cooler He I and O V lines. The value of the non-thermal electron flux ($\geq 3 \times 10^{10}$ ergs cm⁻² s⁻¹) and the resulting velocity response are indicative of an explosive evaporation process occurring during this flare, as laid out in Fisher, Canfield & McClymont (1985a) and Mariska, Emslie, & Li (1989).

The combination of HXR and EUV observations presented in this *Letter* have enabled us to obtain a greater understanding of the characteristics of chromospheric evaporation, a fundamental process in solar flares. We have presented the first detection of explosive mass motions within HXR footpoints, and determined the flux of non-thermal electrons responsible for driving such flows.

This work has been supported by a Department of Employment and Learning (DEL) studentship and a Cooperative Award in Science and Technology (CAST). FPK is grateful to AWE Aldermaston for the award of a William Penny Fellowship. We would like to thank Drs. Brian Dennis, Joe Gurman, and Dominic Zarro at NASA Goddard Space Flight Center for their stimulating discussion and continued support. SOHO is a project of international collaboration between the European

Space Agency (ESA) and NASA.

REFERENCES

- Antiochos, S. K., & Sturrock, P. A., ApJ, 220, 1137
- Antonucci, E., & Dennis, B. R., Sol. Phys., 86, 67
- Brown, J. C., 1971, Sol. Phys., 18, 489
- Czaykowska, A., De Pontieu, B., Alexander, D., & Rank, G., ApJ, 521, L75
- Delaboudiniere, J. -P., et al. 1995, Sol. Phys., 162, 291
- Fisher, G. H., Canfield, R. C., & McClymont, A. N. 1984, ApJ, 281, L79
- Fisher, G. H., Canfield, R. C., & McClymont, A. N. 1985*a*, ApJ, 289, 414
- Fisher, G. H., Canfield, R. C., & McClymont, A. N. 1985*b*, ApJ, 289, 425
- Fisher, G. H., Canfield, R. C., & McClymont, A. N. 1985*c*, ApJ, 289, 434
- Harrison, R. A., et al. 1995, Sol. Phys., 162, 233
- Holman, G. D. 2003, ApJ, 586, 606
- Hurford, G. J., et al. 2002, Sol. Phys., 210, 61
- Lin, R. P., et al. 2002, Sol. Phys., 210, 3
- Mariska, J. T., Emslie, A., G., & Li, P. 1989, ApJ, 341, 1067
- Phillips, K. J. H. 2004, ApJ, 605, 921
- Teriaca, L., Falchi, A., Cauzzi, G., Falciani, R., Smaldone, L. A., & Andretta, V., 2003, ApJ, 588, 596
- Thompson, W. T. 1999, CDS Software Note No. 53
- Zarro, D. M., & Lemen, J. R., 1988, ApJ, 329, 456